# Hybrid Millimeter-Wave Push–Push Oscillators Using Silicon–Germanium HBTs

Franz X. Sinnesbichler, *Member, IEEE*

*Invited Paper*

***Abstract*—Push–push design has proven to be an efficient way to extend the usable frequency range of active devices for oscillator applications. In this paper, the basic principles of push–push oscillator design are explained and various possibilities to realize this concept are shown. Several examples of hybrid millimeter-wave push–push oscillators using SiGe HBTs as active devices are discussed. Details on large-signal modeling of the SiGe HBTs using both a vertical bipolar integrated-circuit model, as well as a customized large-signal model are given. Measured key performance data of microstrip resonator oscillators at 57 and 58 GHz are output power levels of +1 dBm and single-sideband phase-noise figures (1-MHz offset from carrier) of −106 and −108 dBm/Hz, respectively. For the dielectric-resonator oscillators, a maximum output power of −8 dBm and an optimum phase noise of −112 dBc/Hz (−14-dBm output power), as well as a mechanical tuning range of 500 MHz were measured.**

***Index Terms*—Dielectric-resonator oscillator (DRO), harmonic oscillator, large-signal modeling, microstrip oscillator, millimeter-wave circuit, push–push oscillator, silicon–germanium (SiGe) HBT, silicon–germanium (SiGe).**

## I. Introduction

In RECENT years, millimeter-wave systems have become more and more interesting for low-cost applications. This development has mainly been driven by commercial applications, as mobile communications, sensors, etc. [1]. A fundamental precondition for system applications, however, is the realization of suitable signal sources [2]. Applying the push–push principle to oscillator design allows to extend the usable frequency range of active devices for signal-generating applications [3]–[5] and, thus, allows to make use of technologies with relative moderate maximum oscillation frequencies $f_{\max}$ for millimeter-wave applications. This way of using the harmonic signal that is generated inherently in an oscillator has proven to be an efficient way to millimeter-wave oscillator design. In recent time, several push–push oscillators with oscillation frequencies far beyond 100 GHz have been published [4], [6], [7]. A triple-push concept has also been realized [8]. In addition, although this should be verified for different design approaches, there are hints that push–push oscillators may be realized with smaller dimensions and with a lower phase noise compared to solutions using fundamental oscillators combined with frequency multipliers [9], [10]. A further advantage of push–push design is that, due to the separation of internal and external frequency, load pulling can be effectively suppressed by simple methods.

The drawback of push–push oscillators is, however, a more complicated design. The circuit principle usually requires a large-signal analysis to verify the odd-mode operation of the sub-circuits and the bias network has to be properly designed with respect to two critical frequencies.

In the following, the basic principle of push–push oscillators is first explained and some different possibilities of how the concept can be realized are then explained (Section II). Some details on the calculation of even- and odd-mode impedances are also given. Several experimental design studies to demonstrate push–push oscillator performance in the $V$-band are discussed in this paper. As active devices, silicon–germanium HBTs (SiGe HBTs) are used. Due to the immense advances that have been made in SiGe technology during the last years, SiGe HBTs have become very promising devices for applications at microwave- and millimeter-wave frequencies [11], [12]. Further details on the HBTs used in this study are given in Section III. Section IV deals with large-signal modeling of the active devices. Both an approach using a standard model, available in the public domain, as well as an approach using a customized large-signal model are described. In Sections V and VI, as already mentioned, various push–push oscillators are then discussed and experimental results are given.

## II. Push–Push Principle

In general, a push–push oscillator consists of two symmetric sub-circuits (Fig. 1) [13]. Each of those sub-networks is designed to oscillate at half the output frequency of the overall circuit, i.e., at the frequency $f_0 = 1/2f_{\text{out}}$.

The two signals

$$\underline{s}_1(t) = a_1 e^{j\omega_0 t} + a_2 e^{j2\omega_0 t} + a_3 e^{j3\omega_0 t} + \cdots \tag{1}$$

and

$$\underline{s}_2(t) = a_1 e^{j\omega_0 (t-\Delta t)} + a_2 e^{j2\omega_0 (t-\Delta t)} + a_3 e^{j3\omega_0 (t-\Delta t)} + \cdots \tag{2}$$

Manuscript received October 2, 2001; revised April 29, 2002.

The author was with the Lehrstuhl fuer Hochfrequenztechnik, Technische Universität München, 80333 Munich, Germany. He is now with TriQuint Semiconductor GmbH, D-81829 Munich, Germany (e-mail: FSinnesbichler@tqs.com).

Digital Object Identifier 10.1109/TMTT.2002.807836

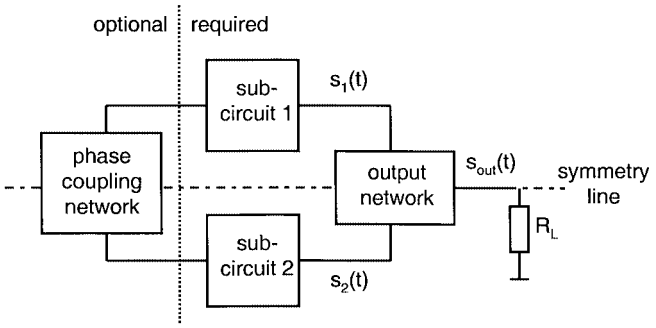


Fig. 1. Principle schematic of a push–push oscillator.

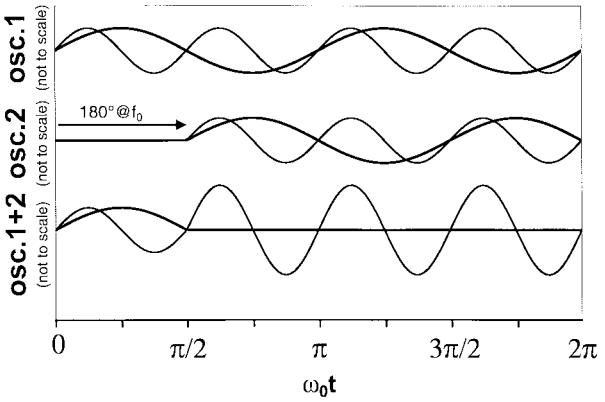


Fig. 2. Addition of two signals in a push–push oscillator.

are added in an appropriate output network to

$$\underline{s}_{\text{out}}(t) = a_1 e^{j\omega_0 t} \cdot \left(1 + e^{-j\omega_0 \Delta t}\right) + a_2 e^{j2\omega_0 t} \cdot \left(1 + e^{-j2\omega_0 \Delta t}\right) + a_3 e^{j3\omega_0 t} \cdot \left(1 + e^{-j3\omega_0 \Delta t}\right) + \cdots. \quad (3)$$

If a phase difference of

$$\omega_0 \cdot \Delta t = \pi \quad (4)$$

at the fundamental frequency is enforced between $\underline{s}_1$ and $\underline{s}_2$, the output signal becomes

$$\underline{s}_{\text{out}}(t) = 2 \cdot a_2 e^{j2\omega_0 t} + 2 \cdot a_4 e^{j4\omega_0 t} + 2 \cdot a_6 e^{j6\omega_0 t} + \cdots \quad (5)$$

where all odd harmonics, especially the fundamental signal, cancel themselves out, whereas the even harmonics are added constructively. Fig. 2 shows a qualitative sketch of this signal addition for the fundamental and first harmonic signal.

Proper design of the oscillator sub-circuits requires knowledge of the impedances provided by the connecting networks for the case of an odd-mode oscillation (and possibly also for the case of an unwanted even-mode oscillation) of the overall circuit. Methods to calculate these impedances are, for example, separating the circuit at the symmetry line and inserting virtual ground nodes for the odd mode and virtual open circuits for the even mode [14] or to perform ac simulations with coupled sources connected to the different ports of the circuit [32].

There are various possibilities to assure the previously mentioned required phase difference of the two sub-circuits.

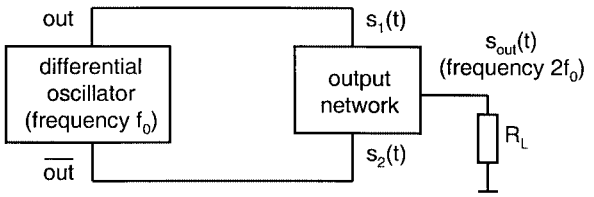


Fig. 3. Push–push oscillator based on a differential oscillator.

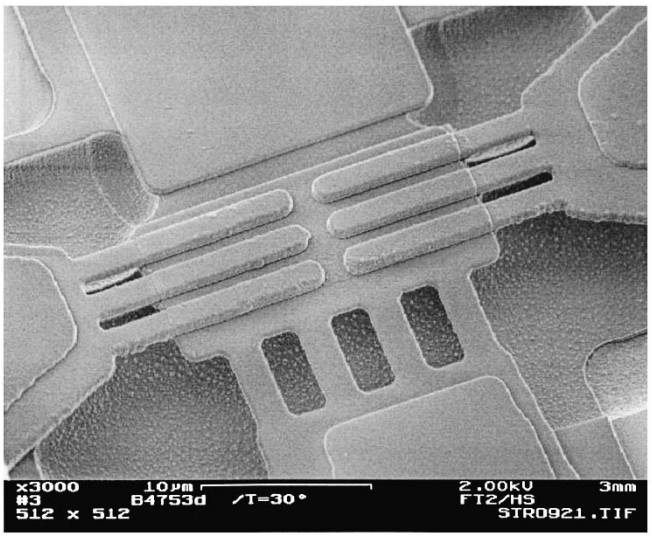


Fig. 4. Microphotograph of the six-finger DaimlerChrysler SiGe HBT.

One procedure is to enforce the phase difference using an appropriate phase-coupling network (Fig. 1). This can be, for example, double-sided microstrip resonators [15]–[18] or dielectric resonators (DRs) [14], [19], [20], as well as appropriate transmission lines [13], [4]. Another possibility is to design the impedances of the connecting output network in such a way that the conditions for oscillation are fulfilled for the odd-mode impedance only, but not for the even-mode impedance [4], [6], [10], [21], [22]. The phase-coupling network shown in Fig. 1 is obsolete in this case.

A somewhat different approach to design a push–push oscillator does not use two separate sub-circuits [7]. Instead, the two output signals $\mathrm{out}$ and $\overline{\mathrm{out}}$ of a differential oscillator are combined (Fig. 3). This approach, however, will not be considered here.

In the following, we will focus on push–push oscillators using microstrip lines and DRs as phase-coupling networks.

## III. Technology

For the oscillators that will be discussed below, two similar types of double-mesa SiGe HBTs are used as active devices. The HBTs have been fabricated at the DaimlerChrysler Research Center, Ulm, Germany [23]–[25]. The devices have two and six emitter fingers with active areas of together 16 $\mu$m$^2$ and 48 $\mu$m$^2$, respectively. Approximate maximum values of $f_T$ and $f_{\max}$ are 40 and 70 GHz for the smaller devices and 45 and 85 GHz for the larger ones. Fig. 4 shows a microphotograph of the six-finger device [26].

The oscillators are fabricated in hybrid thin-film technology on alumina substrates. The HBTs are flip-chip bonded to minimize parasitic inductances and to improve symmetry of the overall circuit and, thus, suppression of the fundamental signal. Similar designs may be realized monolithically integrated on high-resistivity silicon substrates.

## IV. Large-Signal Modeling

Effective design of nonlinear circuits requires accurate large-signal models. Although some basic design steps can be done based on small-signal simulations, a lot of information can only be obtained from large-signal simulations. This includes, for example, output power and exact oscillation frequency. Information on the mode of oscillation of a push–push oscillator, i.e., even or odd mode, can also usually be obtained at best from large-signal simulations.

To obtain suitable models, two different approaches have been followed in this study. In a first step, model parameters have been extracted for a vertical bipolar integrated circuit (VBIC) model [27], [28]. This model, which was proposed in 1995, is mainly based on the well-known SPICE Gummel–Poon (SGP) model [29]. However, several important changes and extensions to the SGP model allow to cover many important characteristics of modern devices. Due to its similarity to the SGP model, the VBIC model is well understood and widely accepted. A key advantage is that it has been implemented in many commercially available circuit simulation programs. Although the VBIC model was originally not intended to model SiGe HBTs, very satisfying results could be obtained for our purposes [30]. To describe the HBTs, the four-terminal model is reduced to a three-terminal version by choosing appropriate parameter values. A later model release now allows to directly choose between a three- and four-terminal version of the VBIC model. To deal with parasitic elements, the model is embedded into a network of parasitic capacitances, inductances, and conductances. Large-signal parameters are extracted from dc and bias-dependent $S$-parameters. Special focus is also given on the modeling of temperature and self-heating effects.

To further improve modeling accuracy, in a more elaborate approach, a novel SiGe HBT large-signal model has been developed and model parameters have been extracted for the six-finger device [31]. As with most modern bipolar transistor models, this model is based on the SGP model. A complete description and a set of model equations can be found in [32]. Fig. 5 shows the equivalent circuit of the model, which consists of the fundamental transistor part, as well as sub-circuits to model self-heating and excess phase behavior [28].

Similar to the Gummel–Poon model, the transport current

$$I_{CC} = \frac{I_f - I_r}{q_b} \tag{6}$$

is connected to the stored charge $q_b$. To take into account the different effective band-gap values of HBTs, however, a generalized version of the integral charge control relation [33] is used to calculate $q_b = q_1 + q_2$. The term

$$q_1 = \frac{Q_{p0} + HJE \cdot Q_{je} + HJC \cdot Q_{jc}}{Q_{p0}} \tag{7}$$

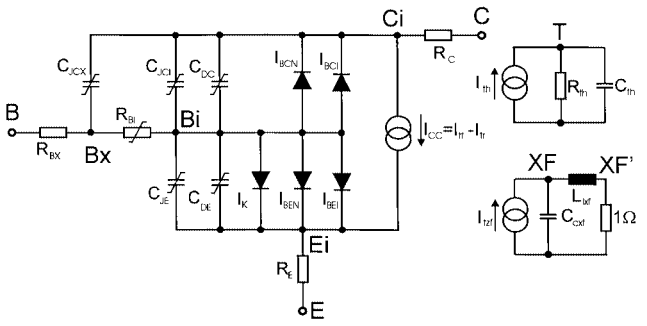


Fig. 5. Equivalent circuit of the large-signal model.

models base-width modulation, whereas

$$q_2 = \frac{HE \cdot Q_{fe} + HC \cdot f_c \cdot Q_{fc} + Q_{f0} + Q_{fb}}{Q_{p0}} \tag{8}$$

models charges stored due to normal forward operation, high-level injection, and the Kirk effect. The coefficients $HJE$, $HJC$, $HE$, and $HC$ have been introduced similar to the HICUM model [34]. Additionally, an empirical smoothing function

$$f_c = \left(\frac{V_{ce}}{VHC}\right)^{-NHC} \tag{9}$$

which defaults to $f_c = 1$, has been introduced to facilitate dc modeling at low collector–emitter voltages. The forward charge components are calculated according to the model proposed by Schroeter and Lee [35]. The base and collector contributions are separated empirically. Due to the dependence of the charges on the collector current, an explicit solution for the transport current (as, for example, in the SGP model) cannot be given. However, as a tradeoff to the very well-suited transit time formulation, an implicit calculation of the transport current can easily be accepted. According to the charge model that has been implemented, as a first quantity, the bias-dependent transit times have to be modeled, followed by the extraction of the dc parameters. A real verification of the charge model, i.e., a comparison of calculated transit frequencies or $S$-parameters to measured values, is only possible after the complete extraction of dc model parameters has been finished. Therefore, any refinement of the transit time parameters results in a large iteration loop for the parameter extraction. To overcome this difficulty, additional model parameters are introduced to fine tune the transit time model without changing the yet determined dc model. These parameters are again optional and can easily be omitted.

The base currents, both in the forward, as well as reverse direction, consist of ideal and nonideal portions. Each of them is modeled using a separate saturation current and emission coefficient. At high currents, the electrical behavior of the devices is dominated by the Kirk effect. Due to the second band-gap discontinuity, this effect is especially pronounced in double HBTs (DHBTs) (as, for example, in SiGe HBTs) [36]. In addition to a strong decrease of the transit frequency due to the stored charge, a severe increase of the base current

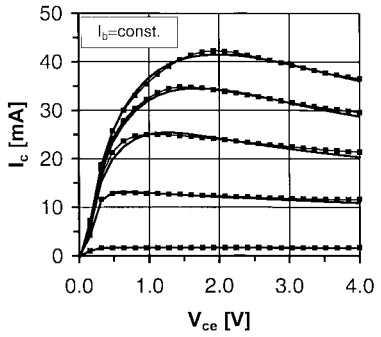


Fig. 6. Measured (dots) and simulated (lines) forward output characteristic at constant base currents.

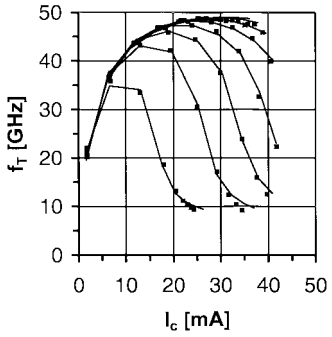


Fig. 7. Measured (dots) and simulated (lines) transit frequencies.

can be observed. This is addressed by an additional current contribution

$$I_K = I_{sK} \cdot \frac{Q_{fc}}{Q_{p0}} \cdot f_K \cdot \left( e^{V_{bei}/n_{beK} \cdot V_T} - 1 \right) \qquad (10)$$

that is directly correlated to the stored charge due to the Kirk effect. The function $f_K = f_K(V_{ce})$ is defined in analogy to (9) and is again used to facilitate the modeling procedure. Using the default parameter values, i.e., $f_c \equiv f_K \equiv 1$, almost identical modeling results can be achieved. However, some more effort then has to be spent on parameter extraction. The junction capacitances are modeled according to the standard SPICE formulation [29] using a linear approximation for voltages $V > FC \cdot V_j$. The base–collector capacitance is separated into the internal and external portions $C_{JCI}$ and $C_{JCX}$, respectively (Fig. 5). The temperature dependencies of the model are implemented similar to the VBIC model [28]. The different saturation currents are modeled according to

$$I_S(T) = I_S(T_0) \cdot \left( \left( \frac{T}{T_0} \right)^x \cdot \exp\left( -\frac{E_g \cdot (1 - T/T_0)}{v_T} \right) \right)^{1/n} \qquad (11)$$

with individual band-gap values for the different materials of the various transistor regions.

Fig. 6 shows a comparison of a measured and simulated output characteristic at room temperature. An excellent fit over the entire range of bias conditions has been achieved. From the part with a negative slope of the current with respect to the voltage, it can be seen that the self-heating behavior is also modeled properly. Accurate temperature dependence has been verified up to 110 °C. Measurements with a forced base–emitter voltage show a positive electrothermal feedback instead of the negative feedback of Fig. 6. This property is also well modeled. The same holds for forward and reverse Gummel plots, as well as the output conductance of the devices.

Finally, the ac model is verified by the excellent agreement of measured and simulated transit frequencies (Fig. 7) and $S$-parameters (Fig. 8) over the entire range of bias conditions. More details on the large-signal model, as well on parameter extraction are given in [31] and [32].

Both of the above-described active device-modeling approaches have been successfully used for circuit designs. The most accurate results with respect to an agreement of simulated and measured data, however, have been achieved using the novel large-signal model.

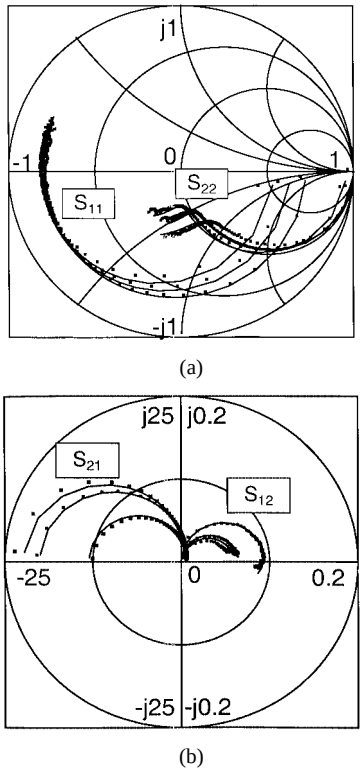


Fig. 8. Measured (dots) and simulated (lines) $S$-parameters ($V_{ce}/I_c$ = 2 V/6.4 mA, 2 V/30 mA, 3 V/17.3 mA, $f = 0.5, \ldots, 40$ GHz).

## V. Microstrip Resonator Oscillators

Various oscillators have been built using microstrip transmission lines as phase-coupling networks. In the following, two of those oscillators will be explained in detail and key performance data will be compared to published oscillator data (see Table I).

The design of the circuits was performed using a commercial microwave design tool. We found out, however, that the simulated frequency response of the provided models for passive elements (as, for example, transmission lines and open stubs) is not precise enough to predict the oscillation frequency with satisfying accuracy. Therefore, during the design process, the frequency response of the passive parts of the layout had to be calculated using a two-dimensional (2-D) field solver (HP Momentum). The excellent agreement of measured oscillator frequencies with simulation results using this approach has been proven by several designs. Since this is a quite time-consuming process, especially at very high frequencies, a mixed design

TABLE I
COMPARISON OF OSCILLATOR PERFORMANCE

| | technology | $f_0$ [GHz] | $P_0$ [dBm] | $L_{ssb}$ (100 kHz) [dBc/Hz] | $L_{ssb}$ (1 MHz) [dBc/Hz] | VCO |
|---|---|---|---|---|---|---|
| Schott [22] | InGaP/GaAs HBT | 38 | -25 | -89 | - | no |
| Huei-Wang [41] | InP-HBT | 40 | 5 | -84 | -111 | no |
| Smith [21] | GaAs/AlGaAs-HBTs | 40 | -27 | -65 | - | yes |
| Ikematsu [42] | AlGaAs/InGaAs-HEMT | 42 | -4.3 | - | -84 | yes |
| Schwarz [43] | InP-HBT | 43 | -3.5 | - | -100 | yes |
| Rheinfelder [44] | SiGe-HBT | 47 | 13 | -99 | - | no |
| Funabashi [45] | AlGaAs/InGaAs-HFET | 50 | 4.5 | -60 | -97 | yes |
| Kashiwa [46] | AlGaAs/InGaAs-HEMT | 56 | 11 | -85 | -103 | no |
| **this work** | **SiGe-HBT** | **57** | **1** | **-** | **-106** | **no** |
| **this work** | **SiGe-HBT** | **58** | **1** | **-83** | **-108** | **no** |
| Kawasaki [47] | InGaP/InGaAs/GaAs-HEMT | 60 | 6.7 | -63 | -87 | no |
| Huei-Wang [41] | InP-HBT | 62 | 4 | -78 | -105 | no |
| Aoki [48] | AlGaAs-HBT | 80 | -9 | - | -80 | no |
| Kudszus [49] | AlGaAs/InGaAs/GaAs-HEMT | 94 | 2 | - | -71 | yes |

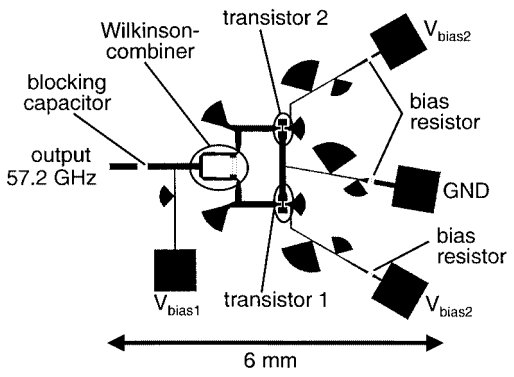


Fig. 9. Layout of a 57-GHz SiGe HBT push–push oscillator.

strategy using both the provided models, as well as full-wave analysis was performed. Simulation of output power is more difficult. The results also vary considerably between simulations using microstrip models and simulations using the results of full-wave analysis to calculate the frequency response of the passive components. In this case, however, a general decision, which type of simulation has to be used, cannot be given. During the design process, the actual simulation results were, therefore, assumed to be somewhere in between the results given by the different treatments of the passive circuit components.

Fig. 9 shows the layout of a 57-GHz oscillator [37]. The circuit is fabricated on a 5-mil alumina substrate using the previously described six-finger devices.

To add the two internal signals, a Wilkinson combiner is designed for operation at $f_{\text{out}} = 2f_0$. The output signal is decoupled from the internal oscillator via a beam-lead capacitor. Stub

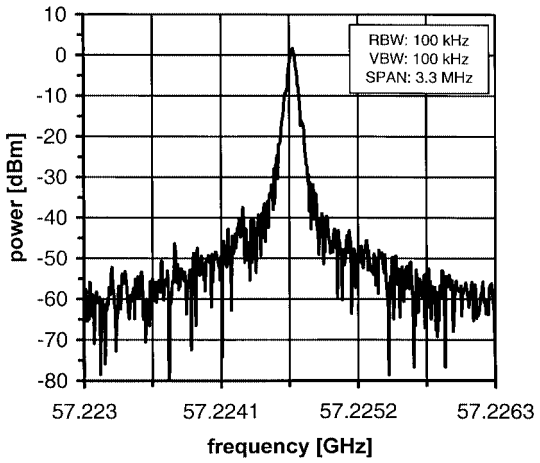


Fig. 10. Typical measured output spectrum of the 57-GHz oscillator.

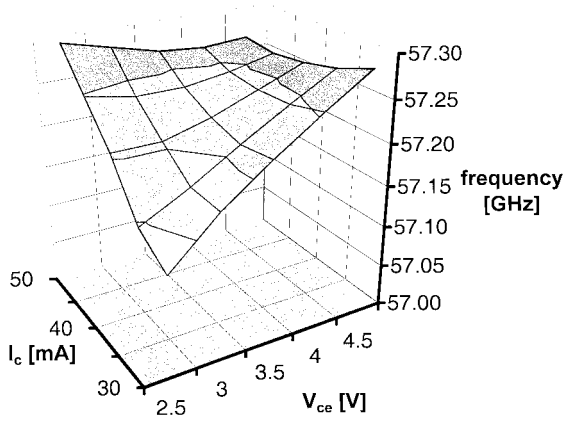


Fig. 11. Measured oscillation frequency of the 57-GHz oscillator versus bias point.

elements designed for 28.5 and 57 GHz, respectively, as well as microstrip transmission-line elements are used to provide the required impedances to the active devices and to decouple the bias feed lines. The correct phase difference between the sub-circuits is enforced by a properly designed microstrip line. First, the electrical length of this line is adjusted to fulfill the overall oscillation condition based on a small-signal analysis. A large-signal analysis is then performed to check for the mode of oscillation. Finally, varying the length of this connecting transmission line by $\lambda/2$ at $f_0$ will shift the oscillator from even to odd mode and vice versa.

A typical measured output spectrum is shown in Fig. 10. According to the selected bias point of the transistors, the oscillation frequency varies between approximately 57.1 and 57.3 GHz (Fig. 11). It can be seen, however, that the dependency of the oscillation frequency on variations of the bias conditions can be minimized by choosing an operating point at a high collector–emitter voltage. The dependency of the output power on the operating point of the transistors is shown in Fig. 12. For maximum output power of the oscillator, an optimum collector current is approximately $I_c = 40$ mA (20 mA through each device). Additionally, the output power of the oscillator is then nearly constant with respect to variations of the collector–emitter voltage.

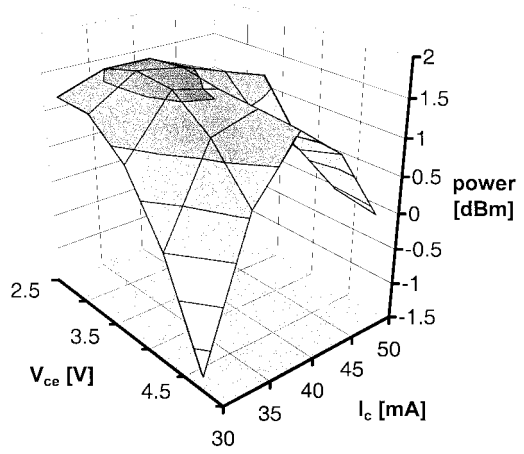


Fig. 12. Measured output power of the 57-GHz oscillator versus bias point.

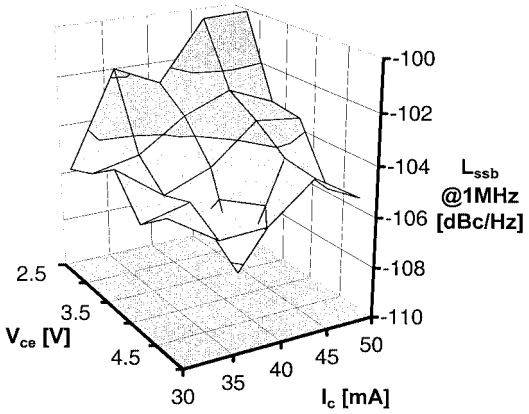


Fig. 13. Measured single-sideband phase noise of the 57-GHz oscillator at an offset frequency of 1 MHz.

For optimum phase noise, a high collector–emitter voltage should be chosen (Fig. 13). Although measured noise data itself is quite noisy, it can clearly be seen that phase noise decreases as the voltage is increased. The single value of $-108$ dBc/Hz at 4 V/40 mA is assumed to be a measurement inaccuracy. Summarizing the results of Figs. 11–13, the optimum performance of this oscillator is achieved at an operating point of $V_{ce} = 4$–$4.5$ V and $I_c = 2\times 20$ mA. An output power of approximately $+1$ dBm and an oscillation frequency of 57.25 GHz are measured. The single-sideband phase noise at an offset frequency of 1 MHz is approximately $-106$ dBc/Hz. Suppression of the fundamental 28.6-GHz signal is $-19$ dBc.

Fig. 14 shows the layout of another oscillator. The circuit is again fabricated on a 5-mil alumina substrate and the transistor chips are flip-chip bonded to minimize bonding inductances. Stub elements are connected to the base terminals of the devices to increase instability. The phase coupling of 180° at $f_0$ is maintained by a microstrip transmission line connecting the collector terminals of the two transistors. To find the correct length of this line, a similar procedure is applied as described for the oscillator above. The respective output signals are again added in a Wilkinson combiner that is optimized for operation at 58 GHz. Finally, the output signal is decoupled via a beam-lead blocking capacitor. The lines for the bias supply voltages are decoupled

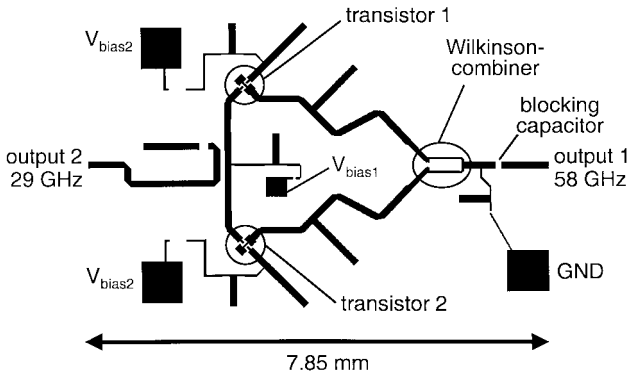


Fig. 14. Layout of the double-frequency oscillator.

by properly positioned stub elements. The operation point of the devices is adjusted using thin-film resistors.

Whereas in this oscillator the collector terminals of the active devices are connected to maintain the required phase difference, in the previously described circuit, the emitter terminals have been connected. For both approaches, the design procedure, as well as the achieved results are similar. Therefore, both topologies may be used and a general decision to prefer one or the other cannot be given.

Via a microstrip coupler, which is added to the phase-coupling network, a portion of the internal 29-GHz signal is coupled out and fed to a second output of the circuit. Future voltage-controlled-oscillator designs may use such an additional output signal at half the frequency of the overall circuit as a reference signal for a phase locked loop (PLL). As a result, the first frequency divider of the PLL can be omitted, allowing a significant simplification of the overall circuit [10]. The fourth terminal of the directional coupler is terminated with a 50-$\Omega$ resistor. The required ground is provided by a $\lambda/4$-stub.

According to the topology described above, several oscillator circuits have been fabricated and characterized [38]. Measured oscillation frequencies are between 58.04–58.4 GHz, which agrees very well with the simulated frequency of 58.2 GHz. Output power of the oscillators is from $-2$ to $+1$ dBm. As already mentioned above, simulated output power levels vary considerably depending on the type of passive models that are used. The simulated range from $-2$ to $+6$ dBm, however, agrees quite well with measured results. Suppression of the fundamental signal at the 58-GHz output is measured to be between 17–27 dBc. Simultaneously, the spectrum at the 29-GHz output is observed. Measured power is between $-2.7$–0 dBm with a suppression of the first harmonic signal between 17.3–26.7 dBc. The difference between these values is caused by varying unsymmetries of the half-circuits due to tolerances in the fabrication of the devices, substrates, and manually attached bonding bumps.

It can be observed that a change in the terminating impedance of any of the two outputs has virtually no influence on the oscillation frequency. This means that, due to the separation of operating frequency $f_0$ and output frequency $f_{\text{out}}$, load pulling is effectively suppressed by an appropriate design of the output network. At offset frequencies of 100 kHz and 1 MHz,

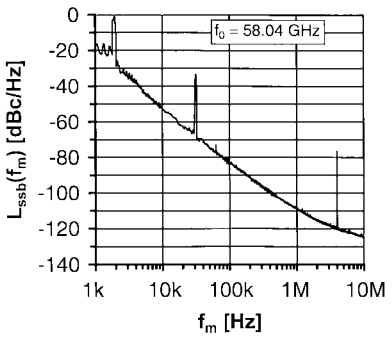


Fig. 15. Measured phase noise of the double-frequency oscillator.

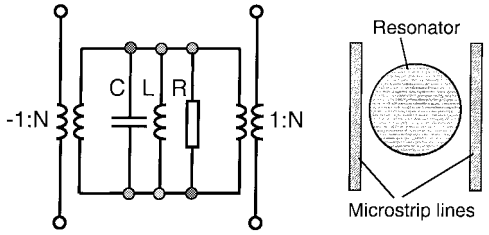


Fig. 16. Equivalent circuit of the DR with two coupling lines.

a single-sideband phase noise of −83 and −108 dBc/Hz has been measured (Fig. 15). The phase noise at the 29-GHz output is approximately 4–5 dB below these values.

## VI. DR Oscillators

Another approach to assure the required phase difference between the sub-circuits of a push–push oscillator is to use a DR. Its magnetic field at the fundamental resonance shows a radial symmetry. Therefore, two transmission lines at two opposite sides of the resonator are coupled with equal magnitude and opposite sign, i.e., with exactly the required phase difference [14], [39].

For the computer-aided design (CAD) of the oscillator, a model of the resonator is required that reflects the odd coupling of the two microstrip lines [40]. Therefore, the *RLC*-equivalent circuit of the resonator is extended with two ideal transformers with response ratios of 1 : N and −1 : N, respectively (Fig. 16). Since the transformers are only used to reflect the odd coupling of the two lines, a value of $N = 1$ is assumed.

Fig. 17 shows the layout of the entire oscillator circuit. On the left-hand side, a beam-lead capacitor is used to decouple the output line from the active circuitry. A modified rat-race coupler is then used as a power combiner (Fig. 18). This element is designed to have high transmission $s_{12}$ and $s_{13}$ from the inputs to the output at 58 GHz. Additionally, it must be symmetric with respect to the two inputs in order to maintain symmetry of the two oscillator half-circuits. As a result, the fourth input of a typical rat-race coupler is omitted. This type of combiner shows slightly higher transmission compared to a Wilkinson combiner and is, therefore, preferred for our application. Additional stubs at the internal output lines of the oscillator are used to improve isolation at 29 GHz. The resonator is coupled to the two transmission lines on the right-hand side of Fig. 17. The lines are terminated with 50-Ω loads to avoid parasitic reflections. The ground of these resistors is provided by $\lambda/4$ stubs at 29 GHz.

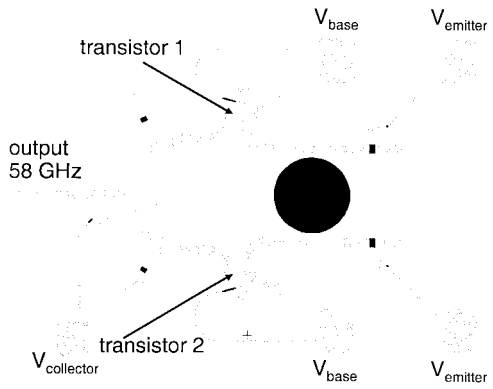


Fig. 17. Layout of the 58-GHz oscillator.

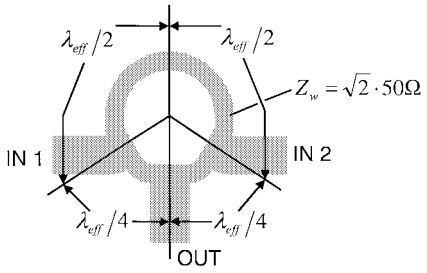


Fig. 18. Layout of the symmetrically modified rat-race coupler.

TABLE II
COMPARISON OF DRO PERFORMANCE

| | technology | $f_0$ [GHz] | $P_0$ [dBm] | $L_{ssb}$ (100 kHz) [dBc/Hz] | $L_{ssb}$ (1 MHz) [dBc/Hz] | VCO |
|---|---|---|---|---|---|---|
| Funabashi [50] | AlGaAs/InGaAs-HFET | 55.1 | 3.7 | -88 | - | no |
| **this work** | **SiGe-HBT** | **58** | **-8**<br>**-14** | **-**<br>**-86** | **-105**<br>**-112** | **no**<br>**no** |
| Inoue [51] | AlGaAs/InGaAs-HFET | 60 | 6.9 | -80 | -104 | yes |
| Wenger [52] | InGaAs/GaAs-HFET | 81 | 0 | - | -90 | no |

At 58 GHz, the lines are then effectively terminated with open circuits, and the power at 58 GHz is reflected. The third terminal of the transistors, in this configuration the base terminal, is connected to open transmission lines to add positive feedback, i.e., to increase instability of the devices. Finally, the bias network mainly uses 58-GHz stubs and proper positioning of the bias lines to decouple dc and ac signals.

Several microstrip oscillator circuits were fabricated in thin-film technology on 10-mil alumina substrates using the smaller two-finger devices. The oscillation frequency is approximately 57.4 GHz with a mechanical tuning range of approximately 500 MHz, i.e., from 57.4 to 57.9 GHz. As expected, a dependence of the output power at 58 GHz on the length of the transmission line between the resonator and terminating 50-Ω resistors was found. A maximum power of −8 dBm was achieved with a phase noise of −105 dBc/Hz at an offset frequency of 1 MHz. Experimentally, we found a tradeoff for circuit optimization between output power and phase noise. With a slightly different line length, resulting in a moderate output power level of approximately −14 dBm, we measured a single-sideband phase noise of −86 and −112 dBc/Hz at offset

frequencies of 100 kHz and 1 MHz, respectively. Suppression of the fundamental signal at 29 GHz was simultaneously measured to be −17 dBc. For a comparison of the performance of these oscillators to the results of the circuits presented in Section V, it should be noted that different types of transistors were used. This influences both output power and phase-noise performance.

Tables I and II show a comparison of key performance data of the presented oscillators to the data of published oscillators at comparable frequencies. The SiGe HBT oscillators of this study, using laboratory samples of the active devices, compare well to the data of oscillators based on GaAs and InP devices.

## VII. Conclusions

The application of the push–push principle to oscillator design allows to extend the usable frequency range of active devices for signal-generating applications. This concept, which makes use of the harmonic signal generated within the oscillator circuit, has been explained and various possibilities of realization have been summarized. SiGe HBTs have been used for design and fabrication of sample oscillators. Details on large-signal modeling of the active devices have been given. Best modeling results have been achieved using a customized large-signal model based on the Gummel–Poon model and including various second-order effects of modern semiconductor devices. Experimental results of both microstrip resonator oscillators, as well as DR oscillators at 57 and 58 GHz have been given. Measured data compares well to the data of published oscillators at similar frequencies.

## Acknowledgment

The author thanks the DaimlerChrysler Research Center, Ulm, Germany, and J.-F. Luy, DaimlerChrysler Research Center for providing the SiGe HBTs. The author also thanks G. R. Olbrich, Technische Universität München, Munich, Germany, and students H. Geltinger, Technische Universität München, B. Hautz, Technische Universität München, and W. Endroess, Technische Universität München, for their contributions to this study.

## References

[1] J.-F. Luy and G. E. Ponchak, "Introduction," *IEEE Trans. Microwave Theory Tech. (Special Issue)*, vol. 46, pp. 569–571, May 1998.

[2] W. Menzel, "Future applications," in *Silicon-Based Millimeter-Wave Devices*, J.-F. Luy and P. Russer, Eds. Berlin, Germany: Springer-Verlag, 1994.

[3] J. R. Bender *et al.*, "Push–push design extends bipolar frequency range," *Microwaves RF*, pp. 91–98, Oct. 1983.

[4] S. Kudszus, W. H. Haydl, A. Tessmann, W. Bronner, and M. Schlechtweg, "Push–push oscillators for 94 and 140 GHz applications using standard pseudomorphic GaAs HEMTs," in *IEEE MTT-S Int. Microwave Symp. Dig.*, 2001, pp. 1571–1574.

[5] F. X. Sinnesbichler, H. Geltinger, and G. R. Olbrich, "A 38 GHz push–push oscillator based on 25 GHz-$f_T$ BJTs," *IEEE Microwave Guided Wave Lett.*, vol. 9, pp. 151–153, Apr. 1999.

[6] K. W. Kobayashi *et al.*, "A 108-GHz InP-HBT monolithic push–push VCO with low phase noise and wide tuning bandwidth," *IEEE J. Solid-State Circuits*, vol. 34, pp. 1225–1232, Sept. 1999.

[7] Y. Baeyens *et al.*, "Compact InP-Based HBT VCOs with a wide tuning range at $W$-and $D$-band," *IEEE Trans. Microwave Theory Tech.*, vol. 48, pp. 2403–2408, Dec. 2001.

[8] Y.-L. Tang and H. Wang, "Triple-push oscillator approach: Theory and experiments," *IEEE J. Solid-State Circuits*, vol. 36, pp. 1472–1479, Oct. 2001.

[9] A.-S. Huyn *et al.*, "$K$-band hair-pin resonator oscillators," in *IEEE MTT-S Int. Microwave Symp. Dig.*, 1999, pp. 725–728.

[10] Y. Sun, T. Tieman, H. Pflug, and W. Velthius, "A fully integrated dual-frequency push–push VCO for 5.2 and 5.8 GHz wireless applications," *Microwave J.*, pp. 64–74, Apr. 2001.

[11] P. Russer, "Si and SiGe millimeter-wave integrated circuits," *IEEE Trans. Microwave Theory Tech.*, vol. 46, pp. 590–603, May 1998.

[12] J. D. Cressler, "SiGe HBT technology: A new contender for Si-based RF and microwave circuit applications," *IEEE Trans. Microwave Theory Tech.*, vol. 46, pp. 572–589, May 1998.

[13] K. Fujii, Y. Hara, and H. Isikawa, "$J$ band GaAs MMIC push–push VCO," in *Asia–Pacific Microwave Conf.*, vol. 1, 1993, pp. 6/20–6/23.

[14] C.-M. Liu and C. Y. Ho, "On the design of a voltage-tuned push–push dielectric resonator oscillator," *Microwave J.*, pp. 165–174, June 1990.

[15] H. Yabuki, M. Sagawa, and M. Makimoto, "Voltage controlled push–push oscillators using miniaturized hairpin resonators," in *IEEE MTT-S Int. Microwave Symp. Dig.*, 1991, pp. 1175–1178.

[16] H. Yabuki, M. Sagawa, and M. Makimoto, "New type of oscipliers for the frequency synthesizer," in *IEEE MTT-S Int. Microwave Symp. Dig.*, 1992, pp. 1085–1088.

[17] A.-S. Hyun *et al.*, "$K$-band hair-pin resonator oscillators," in *IEEE MTT-S Int. Microwave Symp. Dig.*, 1999, pp. 725–728.

[18] L. Dussopt, D. Guillois, and G. M. Rebeiz, "A low phase noise silicon 9 GHz VCO and an 18 GHz push–push oscillator," in *IEEE MTT-S Int. Microwave Symp. Dig.*, 2002, pp. 695–698.

[19] J.-Y. Lee and U.-S. Hong, "Push–push subharmonically injection-locked oscillator," *Electron. Lett.*, vol. 32, no. 19, pp. 1792–1793, Sept. 1996.

[20] I. S. Kim, C. Jo, and Y. Han, "Output power improvement of a push–push FET DRO by using an additional DR," *Microwave J.*, pp. 104–107, Apr. 2002.

[21] D. M. Smith, J. C. Canyon, and D. L. Tait, "25–42 GHz GaAs heterojunction bipolar transistor low phase noise push–push VCOs," in *IEEE MTT-S Int. Microwave Symp. Dig.*, 1989, pp. 725–728.

[22] M. Schott, H. Kuhnert, J. Hilsenbeck, J. Würfl, and H. Heinrich, "38 GHz push–push GaAs-HBT MMIC oscillator," in *IEEE MTT-S Int. Microwave Symp. Dig.*, 2002, pp. 839–842.

[23] E. Kasper, H. Kibbel, H.-J. Herzog, and A. Gruhle, "Growth of 100 GHz SiGe heterojunction bipolar transistor (HBT) structures," *Jpn. J. Appl. Phys.*, vol. 33, pp. 2415–2418, 1994.

[24] A. Gruhle, "SiGe heterojunction bipolar transistors," in *Silicon-Based Millimeter-Wave Devices*, J.-F. Luy and P. Russer, Eds. Berlin, Germany: Springer, 1994.

[25] K. M. Strohm, J.-F. Luy, F Schäffler, H. Jorke, H. Kibbel, C. Rheinfelder, R. Doerner, J. Gerdes, F. J. Schmückle, and W. Heinrich, "Coplanar $Ka$-band SiGe-MMIC amplifier," *Electron. Lett.*, vol. 33, no. 16, pp. 1353–1354, Aug. 1995.

[26] M. M. Kaleja, A. Grübl, F. X. Sinnesbichler, G. R. Olbrich, K. M. Strohm, J.-F. Luy, and E. M. Biebl, "Application of Si/SiGe HBT's in active integrated antennas," in *IEEE MTT-S Silicon Monolithic Integrated Circuits in RF Systems Symp.*, Garmisch, Germany, Apr. 26–28, 2000, pp. 64–66.

[27] C. C. McAndrew *et al.*, "VBIC95: An improved vertical, IC bipolar transistor model," in *Proc. BiCMOS Circuits and Technology Meeting*, Minneapolis, MN, 1995, pp. 170–177.

[28] C. C. McAndrew *et al.*, "VBIC95, the vertical bipolar inter-company model," *IEEE J. Solid-State Circuits*, vol. 31, pp. 1476–1483, Oct. 1996.

[29] G. Massobrio and P. Antognietti, *Semiconductor Device Modeling With SPICE*, 2nd ed. New York: McGraw-Hill, 1993.

[30] F. X. Sinnesbichler and G. R. Olbrich, "Electro-thermal large-signal modeling of SiGe HBTs," in *Proc. 29th Eur. Microwave Conf.*, vol. II, Munich, Germany, Oct. 1999, pp. 125–128.

[31] F. X. Sinnesbichler and G. R. Olbrich, "Accurate large-signal modeling of SiGe HBTs," in *IEEE MTT-S Int. Microwave Symp. Dig.*, Boston, MA, June 2002, pp. 749–752.

[32] F. X. Sinnesbichler, *Großsignalmodellierung von SiGe-Heterobipolartransistoren für den Entwurf von Millimeterwellenschaltungen* (in German). Düsseldorf, Germany: VDI Verlag, 2000.

[33] M. Schroeter, M. Friedrich, and H.-M. Rein, "A generalized charge-control relation and its application to compact models for silicon based HBT's," *IEEE Trans. Electron Devices*, vol. 40, pp. 2036–2046, Nov. 1993.

[34] M. Schroeter. HICUM/Level2 model equations. [Online]. Available: http://www.iee.et.tu-dresden.de/iee/eb/comp_mod.html.

[35] M. Schroeter and T.-Y. Lee, "Physics-based minority charge and transit time modeling for bipolar transistors," *IEEE Trans. Electron Devices*, vol. ED-46, pp. 288–300, Feb. 1999.
[36] A. J. Joseph, J. D. Cressler, D. M. Richey, and G. Niu, "Optimization of SiGe HBT's for operation at high current densities," *IEEE Trans. Electron Devices*, vol. 46, pp. 1347–1354, July 1999.
[37] F. X. Sinnesbichler and G. R. Olbrich, "SiGe HBT push–push oscillators for $V$-band operation," in *IEEE MTT-S Silicon Monolithic Integrated Circuits in RF Systems Symp.*, Garmisch, Germany, Apr. 26–28, 2000, pp. 55–59.
[38] F. X. Sinnesbichler, B. Hautz, and G. R. Olbrich, "Low phase noise 58 GHz SiGe HBT push–push oscillator with simultaneous 29 GHz output," in *IEEE MTT-S Int. Microwave Symp. Dig.*, Boston, MA, June 2000, pp. 35–38.
[39] A. M. Pavio and M. A. Smith, "Push–push dielectric resonator oscillator," in *IEEE MTT-S Int. Microwave Symp. Dig.*, 1985, pp. 266–269.
[40] F. X. Sinnesbichler, B. Hautz, and G. R. Olbrich, "A Si/SiGe HBT dielectric resonator push–push oscillator at 58 GHz," *IEEE Microwave Guided Wave Lett.*, vol. 10, pp. 145–147, Apr. 2000.
[41] H. Wang *et al.*, "Low phase noise millimeter-wave frequency sources using InP-based HBT MMIC technology," *IEEE J. Solid-State Circuits*, vol. 31, pp. 1419–1425, Oct. 1996.
[42] H. Ikematsu, K. Kawakami, T. Katoh, and K. Itoh, "A 40 GHz-band fully monolithic VCO with a one-wave length microstrip resonator for accurate oscillation frequency," in *IEEE MTT-S Int. Microwave Symp. Dig.*, 2002, pp. 843–846.
[43] V. Schwarz, T. Morf, A. Huber, H. Jackel, and H. R. Benedicter, "Differential current controlled *LC* oscillators with frequencies of 43 and 67 GHz," *Electron. Lett.*, vol. 35, no. 14, pp. 1197–1198, July 1999.
[44] C. N. Rheinfelder, K. M. Strohm, L. Metzger, H. Kibbel, J.-F. Luy, and W. Heinrich, "47 GHz SiGe-MMIC oscillator," in *IEEE MTT-S Int. Microwave Symp. Dig.*, 1999, pp. 5–8.
[45] M. Funabashi, K. Ohata, K. Onda, T. Inoue, K. Hosoya, K. Maruhashi, and M. Kuzuhara, "Millimeter-wave AlGaAs/InGaAs heterojunction finite-element monolithic microwave integrated circuit oscillators," in *Electronic Communications Jpn.*, vol. 78, May 1995, pp. 49–56.
[46] T. Kashiwa, T. Ishida, T. Katoh, H. Kurusu, H. Hoshi, and Y. Mitsui, "$V$-band high-power low phase-noise monolithic oscillators and investigations of low phase-noise performance high drain bias," *IEEE Trans. Microwave Theory Tech.*, vol. 46, pp. 1559–1565, Oct. 1998.
[47] Y. Kawasaki, K. Shirikawa, Y. Ohashi, and T. Saito, "60 GHz monolithic oscillator using InGaP/InGaAs/GaAs HEMT technology," in *IEEE MTT-S Int. Microwave Symp. Dig.*, 1995, pp. 541–544.
[48] T. Aoki, K. Tezuka, H. Matsuura, S. Kobayashi, T. Fujita, and A. Miura, "80 GHz AlGaAs HBT oscillator," in *18th Annu. IEEE GaAs IC Symp.*, 1996, pp. 281–284.
[49] S. Kudszus, W. H. Haydl, M. Neumann, A. Bangert, and A. Hulsmann, "Subharmonically injection locked 94 GHz MMIC HEMT oscillator using coplanar technology," in *IEEE MTT-S Int. Microwave Symp. Dig.*, 1998, pp. 1585–1588.
[50] M. Funabashi, K. Ohata, K. Onda, K. Hosoya, T. Inoue, M. Kuzuhara, K. Kanckawa, and Y. Kobayashi, "A $V$-band AlGaAs/InGaAs heterojunction FET MMIC dielectric resonator oscillator," in *16th Annu. IEEE GaAs IC Symp.*, 1994, pp. 30–33.
[51] T. Inoue, K. Ohata, L. Funabashi, K. Hosoya, K. Maruhashi, Y. Makino, and M. Kuzuhara, "60 GHz dielectrically stabilized monolithic voltage controlled oscillator," in *25th Eur. Microwave Conf.*, 1995, pp. 281–284.
[52] J. Wenger and U. Güttich, "$Ka$- and $W$-band PM HFET DROs," *IEEE Microwave Guided Wave Lett.*, vol. 3, pp. 191–193, June 1993.

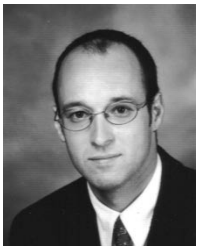

**Franz X. Sinnesbichler** (S'95–A'00–M'01) was born in Rosenheim, Germany, in 1969. He received the Dipl.-Ing. and Dr.-Ing. degrees in electrical engineering from the Technische Universität München, Munich, Germany, in 1995 and 2000, respectively.

From 1995 to 2000, he was with the Lehrstuhl für Hochfrequenztechnik, Technische Universität München, where he was involved with large-signal and noise modeling of field-effect and bipolar devices, as well as the design of millimeter-wave oscillators. In 2000, he joined Infineon Technologies AG, Munich, Germany, where he was involved with the development of GaAs HBT power amplifiers for mobile applications, as well as on low-noise amplifier and mixer applications of high electron-mobility transistor (HEMT) devices. Since 2002, he has been with TriQuint Semiconductor GmbH, Munich, Germany, where he continues to be involved with the development of GaAs power amplifiers and is responsible for various LNA and mixer products.